Medical Engineering and Physics 64 (2019) 46–55

Contents lists available at ScienceDirect

Medical Engineering and Physics

journal homepage: www.elsevier.com/locate/medengphy

A stability-based model of a growing spine with adolescent idiopathic scoliosis: A combination of musculoskeletal and finite element approaches

Zeinab Kamal[a], Gholamreza Rouhi[a,*], Navid Arjmand[b], Samer Adeeb[c]

[a] Department of Biomedical Engineering, Amirkabir University of Technology, Tehran, Iran
[b] Department of Mechanical Engineering, Sharif University of Technology, Tehran, Iran
[c] Department of Civil and Environmental Engineering, University of Alberta, Edmonton, AB, Canada

ARTICLE INFO

Article history:
Received 16 April 2018
Revised 15 December 2018
Accepted 31 December 2018

Keywords:
Adolescent idiopathic scoliosis
Growth modulation
Spine stability
Musculoskeletal model
Finite element analysis

ABSTRACT

Using a combined musculoskeletal and finite element (FE) approach, this study aimed to evaluate stability-based muscle forces in a spine with adolescent idiopathic scoliosis (AIS) as compared to a normal spine; and subsequently, determine the effects of stress distribution on the growth plates (GPs) of the growing spine. For this purpose a nonlinear 3D FE model of one normal and one scoliotic thoracolumbar spine, consisting of GPs attached to rigid L1 to L4 vertebrae, were developed using computed tomography images coupled with a growth modulation using the Stokes' model. Corresponding well with recent *in-vivo* and *in-vitro* studies, results of the models predicted intradiscal pressures at the L3-L4 and L4-L5 levels of 0.32 and 0.38 MPa in the normal spine and 0.30 and 0.36 MPa in the scoliotic spine, respectively; and hydrostatic and octahedral shear stresses on the apical GP of 0.11 and 0.06 MPa, respectively. The reaction moments in the scoliotic model resulted in higher compression on the posteroconcave side of the GPs, which led to deformity progression as predicted by the Hueter–Volkmann theory. Moreover, the augmented baseline growth in the Stokes' model magnified both the scoliotic spine height and Cobb angle growth rates. The presented stability-based approach can be used to predict the performance of rehabilitation strategies in the clinical management of AIS.

1. Introduction

Adolescent idiopathic scoliosis (AIS) is characterized by three-dimensional axial rotation and lateral curvature of the spine, and is the most common type of spine deformity in adolescents ranging from age 10 to 18 years [1,2]. A medical follow-up every 4–6 months is suggested for AIS patients [3]. There have been a number of passive, i.e. devoid of muscles, finite element (FE) models developed to simulate a growing spine with AIS [4–7]. For instance, the effects of multi-axial stresses on deformation of spinal motion segments of an adolescent have been investigated using both energy-based and Stokes' growth models [4]. Using a FE model of the L5-S1 spondylolisthesis, a strong correlation has been found between pelvic incidence and shear/compression stresses in the growth plate (GP) and in the intervertebral disc (IVD) at the junction [5]. Another FE model of a scoliotic spine has been used to investigate the effect of a proposed smart growing rod which can be more easily adjusted to the determined optimum length during growth thus increasing the effectiveness of treatment [6]. A different FE model able to recommend a range of distraction force to use for optimal correction was used to investigate the optimal distraction force of the growing rod on the spine growth and curvatures as well as the stresses on the rod and screws [7].

Since trunk muscles play a crucial role in the kinetics and stability of the spine [8,9], a combined musculoskeletal (MS) and FE model of the scoliotic spine needs to be developed to study the effect of muscle activation/co-activation on the biomechanics of the spine. The effect of muscle forces on L4-L5 load sharing has been previously investigated using a combined MS and FE model of a healthy individual [10]. In a study by Huynh and co-workers [11],

Abbreviations: AIS, Adolescent idiopathic scoliosis; FE, Finite element; NFE, Normal finite element; SFE, Scoliotic finite element; MS, Musculoskeletal; PCSA, Physiological cross-sectional area; GP, Growth plate; IVD, Intervertebral disc; IDP, Intradiscal pressure; CoR, Center of reaction; SD, Standard deviation; CT, Computed tomography; EOS, Electro Optical System; CAD, Computer-aided drawing; LGPT, Longissimus thoracis pars thoracic; LGPL, Longissimus thoracis pars lumborum; ICPT, Iliocostalis lumborum pars thoracic; ICPL, Iliocostalis lumborum pars lumborum; MFL, Multifidus lumborum; MFT, Multifidus thoracis; QL, Quadratus lumborum; IP, Iliopsoas; EO, External oblique; IO, Internal oblique; RA, Rectus abdominus.

* Corresponding author.
E-mail addresses: kamal@aut.ac.ir (Z. Kamal), grouhi@aut.ac.ir, grouhi@uottawa.ca (G. Rouhi), arjmand@sharif.edu (N. Arjmand), adeeb@ualberta.ca (S. Adeeb).

https://doi.org/10.1016/j.medengphy.2018.12.015
1350-4533/

Duchenne muscular dystrophy was simulated by applying unilateral trunk muscle weakness in a MS model of the growing spine. Their FE model consisted of simple rigid masses connected by beam and spring elements representing the intervertebral discs, ligaments, and facet joints [12]. MS models can be employed to estimate muscle forces, and then, with the addition of gravity loads, they can be used in a geometrically-detailed FE model of the spine to determine stress distribution on passive tissues, and ultimately to study the growth of the spinal column or some of its segments. However, stress distribution within a GP under muscle exertions has not yet been investigated in a combined MS-FE model which can integrate growth modulation in the GP of an AIS spine.

In the current literature review, the center of reaction (CoR) was defined to be the geometric center of IVD for a normal spine [12–14], which can cause sagittaly-symmetric stress distribution in the GP leading to normal vertebrae growth and consequently to a normal spine curve [15]. The asymmetric geometry of a scoliotic spine relative to the sagittal plane causes the CoR to deviate from the geometrical center, i.e. centroid of the IVDs. That, in turn, results in additional reaction moments on the IVDs. The off-centered CoR induces reaction moments on those vertebrae that are postulated to cause different bone growth rates due to non-uniform stress distribution on the vertebral body. These non-uniform stress distributions are predicted to lead to progression of the deformity during growth, in accordance with the Hueter–Volkmann theory [15], which states that increased compression and tension on the GPs reduces and accelerates the vertebral growth rate, respectively. The goal of the treatments currently used for AIS deformity, e.g. growing rod, brace, and physiotherapy, is to generate a more uniform stress distibution on the GPs until the patient reaches skeletal maturity. Despite the great importance of the CoR position for spine equilibrium, the effects of the asymmetric geometry of an AIS spine on the CoR and the growth rate in different sections of the GPs remain poorly understood. Therefore, accurate estimation of trunk muscle forces, reaction moments, the position of the CoR in scoliotic vertebrae, and the associated stress distributions on the GPs of scoliotic spines are needed for more accurate predictions of the growth patterns of affected spines.

The present study attempts to use a combined MS-FE modeling approach to evaluate muscle forces and reaction moments in a spine with AIS compared to a normal spine. These forces and moments would allow the determination of the stress distribution within the GPs of the growing spine and, using a proper growth model, could predict growth patterns in healthy and scoliotic spines. In this study, nonlinear 3D FE models of normal and scoliotic thoracolumbar spines with GPs attached to the cranial and caudal surfaces of each rigid L1 to the L4 vertebrae were developed based on subject-specific upright position images. Muscle forces and reaction moments, estimated by the stability-based MS model, along with gravitational forces were prescribed to the subject-specific FE models to calculate the spine curvatures and stress distributions within the GP for a growing spine of both a normal and a scoliotic adolescent. L3-L4 and L4-L5 intradiscal pressures (IDPs) of the normal and scoliotic models, the shift of CoR from the IVD centroids, hydrostatic and octahedral shear stresses in the apical GP, von Mises stress distribution within scoliotic GPs, and the growth velocities of the spine height, frontal scoliotic Cobb and lordosis angles were calculated based on an upright-standing posture. Moreover, sensitivity analyses were performed to assess the likely effects of varying different parameters in the Stokes' model on the vertebral growth rate and progression of curvatures.

2. Materials and method

Two MS models of trunk muscles were established based on the coordinates of the point of attachment of the muscle fascicles. Thereafter, muscle forces and reaction moments, calculated by the MS models, along with gravity loads were prescribed on subject-specific FE models to estimate stress distribution within the GPs of the L1 to the L4 vertebrae. In the following, the details of the FE models are introduced followed by a description of the MS models.

2.1. Finite element models

The computer-aided drawing (CAD) parts of bones were developed based on computed tomography (CT) images (0.6 mm slice thickness) of a thoracolumbar of a child with AIS (11.5 years, 136.4 cm, 31 kg, lumbar lordosis and frontal Cobb angles of 26.2° and 24.4°, respectively, for the left-convex L1-L4 scoliosis curve with an apex at L2) using Mimics (Materialise, V10.01) in the supine posture. Then, using Electro Optical System (EOS) imaging software (EOS imaging Co., France, Stereo Radiographic Patient Imaging) [22], EOS images of the same scoliotic trunk were used to re-align the CAD parts of the vertebrae to have similar inclinations in the anatomical planes to the upright-standing position (Fig. 1). Deformities of the upright scoliotic spine were considered in all anatomical planes (Fig. 1). Since the bony structures of a lumbar spine with a scoliotic Cobb angle less than 30° has no wedging in the primary stages of deformity initiation [23], the CAD parts of bones of the scoliotic model were re-aligned using EOS images of an adolescent with a normal healthy trunk (11years, 136.1 cm, 30.5 kg, and L1-L4 lumbar lordosis angle of 26°) to create a normal model of the spine in an upright-standing position (Fig. 1). This study was approved by Shahid Sadooghi Hospital (Yazd, Iran) and the informed consent was obtained from both subjects.

Subsequently, growth plates, which were created parallel to the outer surfaces of the caudal and cranial endplates of L1 to the L4 vertebrae [24], were developed in Catia (Dassault Systèmes®, Vélizy-Villacoublay, France, V5R20) (Fig. 1e). To analyze the scoliotic FE (SFE) and normal FE (NFE) models, the CAD parts of the bones and the GPs were imported into computer-aided engineering software (ABAQUS 6.10, ABAQUS Inc., Providence, RI, USA). The GPs were modelled having three distinct parts: mineralized (orthotropic material), growth (orthotropic material), and load-sensitive (isotropic material) with respective thicknesses of 0.3, 0.5, and 0.3 mm [4]. All bony structures and the entire thorax were assumed to be rigid [25–31] and were assigned the element type of R3D4. All areas of each GP were modeled with three-dimensional, 8-nodal reduced integration hexahedron solid elements (C3D8R) with relative mapping between the FE model elements of load-sensitive and growth areas of the GPs [4] (Fig. 1). Since the only function of the bone elements in the current models was for visualization of the bone surfaces and confirmation of correct soft tissue attachments, all bony parts were considered fully-constrained in static analyses (Fig. 1e).

The reaction forces (F^{CoR}) and reaction moments (M^{CoR}) about each IVD centroid were estimated according to static equilibrium (Fig. 1e). Material properties of the GP components were extracted from the literature [24,32] (Table 1).

2.2. Musculoskeletal models

The attachment sites of muscle fascicles to the bones in the FE models were estimated based on parametric anatomical studies of the musculoskeletal spine [16–21] (Fig. 1). To simulate the geometry of the MS model, MATLAB scripting (MATLAB® R2014b, Mathworks Inc., Natick, MA, US) was employed to compute the coordinates of muscle attachment positions in the FE models and curve fitting centered at the vertebrae, which have a total of six IVDs (T12-L1 through L5-S1) each having three non-linear rotational stiffness values [33] (Fig. 2). The distributed gravitational

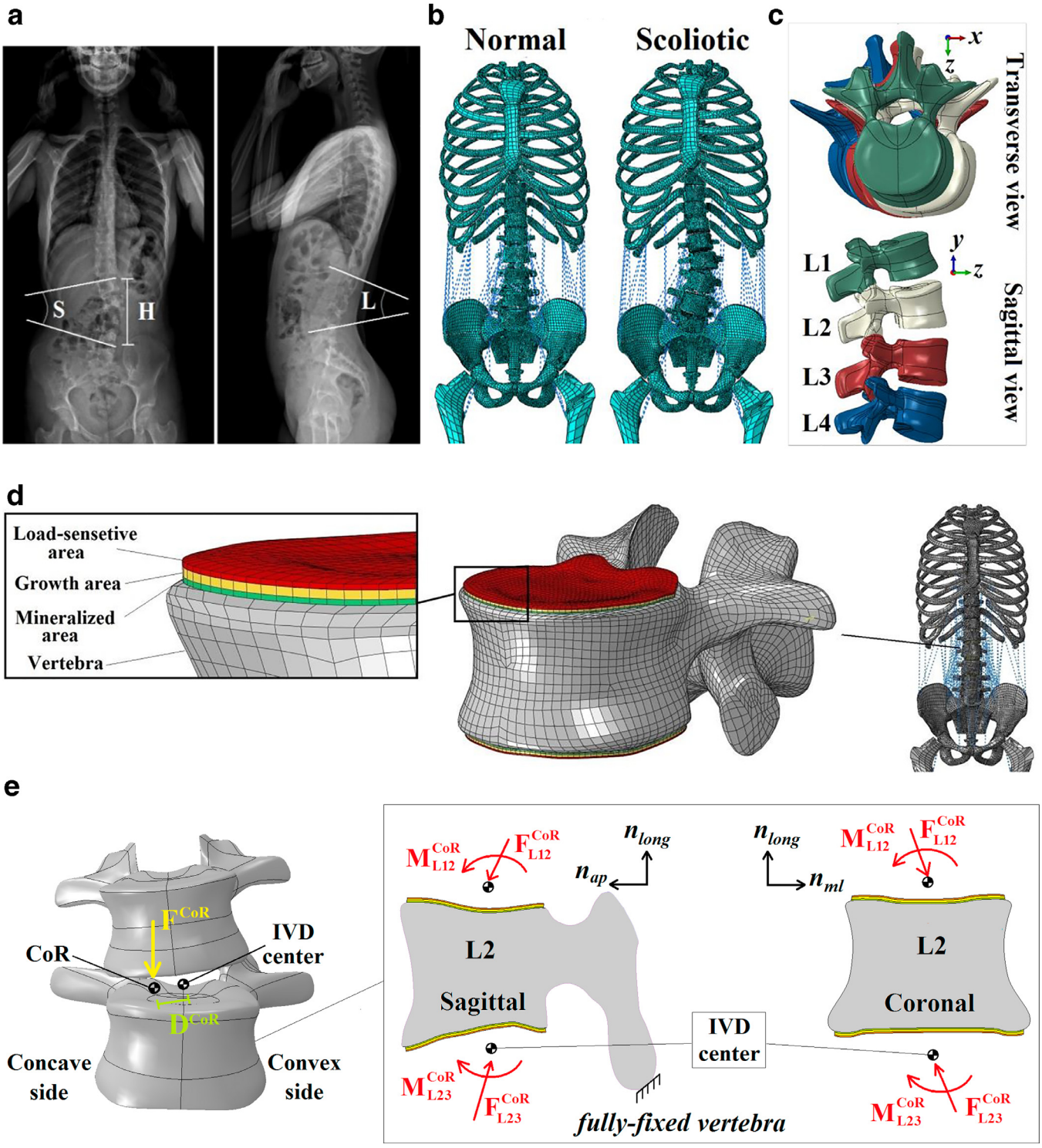

Figure 1. (a) EOS images of the scoliotic spine, in which S, L, and H represents, respectively, the scoliosis frontal Cobb angle, lordosis angle, and height of L1-L4. (b) FE model of: normal and scoliotic thoracolumbar spine (trunk muscles are represented with dashed lines) in frontal view. (c) Model of L1 through L4 of the scoliotic spine in the transverse and sagittal planes. (d) Detailed model of the upper GP of a vertebra in the FE model showing the mineralized, growth, and load-sensitive areas, with their respective thicknesses of 0.3 mm, 0.5 mm, and 0.3 mm [4]. (e) Schematic depiction of reaction force (F^{CoR}) on the CoR, which in the case of scoliosis is shifted about D^{CoR} from the IVD centroid. The reaction moment (M^{CoR}) is the product of F^{CoR} multiplied by D^{CoR}. Free body diagram of a vertebra, here L2 as an example, is illustrated in coronal and sagittal views with the reaction forces and moments about the spinal joints on cranial and caudal GPs. The unit vectors of n_{long}, n_{ml}, and n_{ap}, respectively, are in the local longitudinal, mediolateral, and anteroposterior directions on the GP surface. The reaction moments about the center of IVD (M^{CoR}) consist of the M^{ap}, M^{ml}, and M^{long}, and the shift of CoR positions from the IVD center (D^{CoR}) consist of the D^{ap}, D^{ml}, and D^{long}, respectively, alongside the anteroposterior, mediolateral, and longitudinal directions at each level.

Table 1
Mechanical properties of growth plate components used in the finite element models.

Various parts of growth plate	Young and shear moduli of elasticity (MPa)						Poisson's ratio (v)	Ref.
	E_m	E_n	E_l	G_{nl}	G_{ml}	G_{mn}		
Load-sensitive area	23.8	23.8	23.8	10.6	10.6	10.6	0.4	[32]
Growth area	401	767	1157	24	24	20.4	0.12	[24]
Mineralized area	401	767	1157	24	24	20.4	0.12	[25]

Note that m, n, and l, respectively, are alongside the mediolateral, anteroposterior, and longitudinal directions at each level.

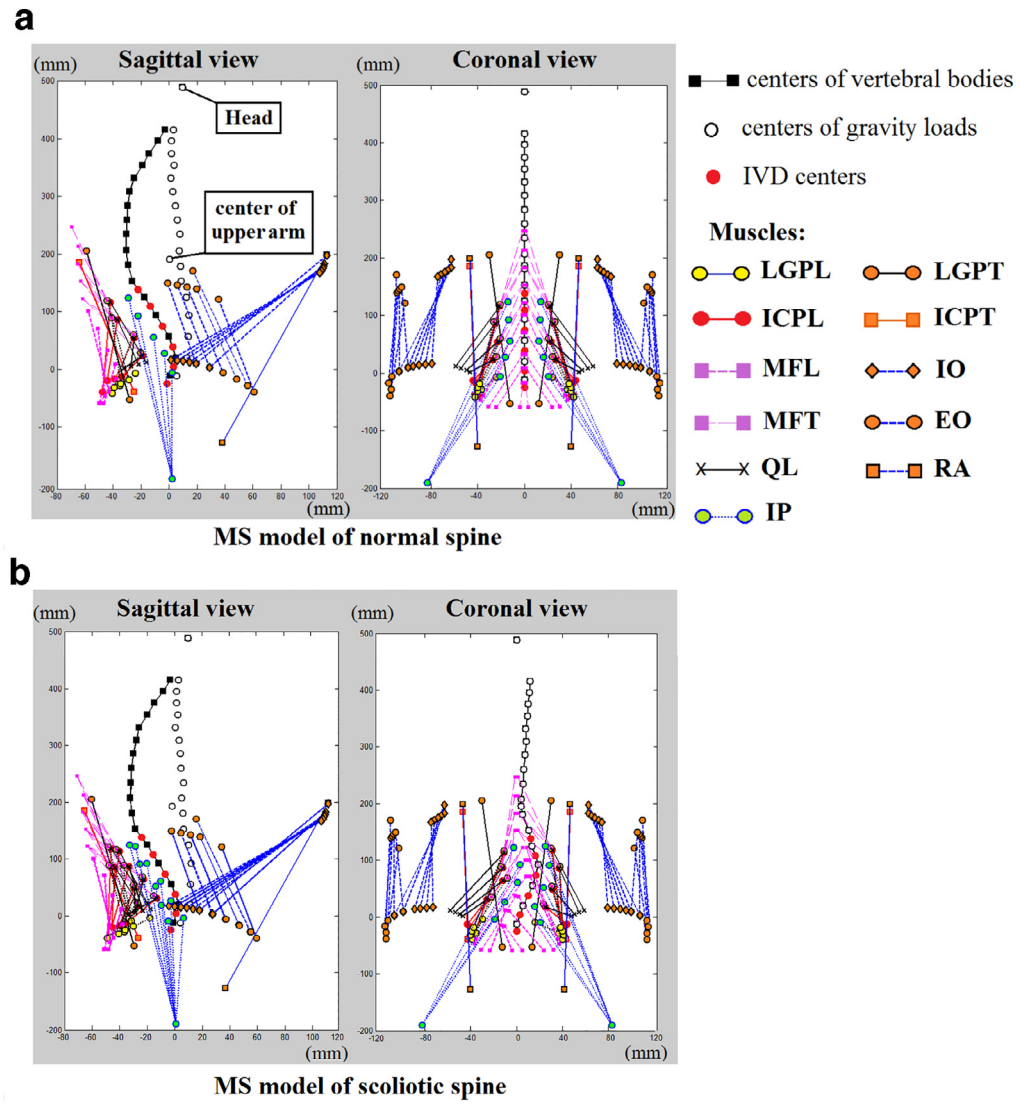

Figure 2. Musculoskeletal models of: (a) a normal; and (b) a scoliotic thoracolumbar spines in the upright-standing posture, in both sagittal and coronal views with center of gravity loads represented as the white circular points in front of the vertebral column. The black squares and red circles in the vertebral column are the position of vertebrae and IVDs, respectively, which were assumed as their geometric centroids [12–14]. Ninety-two bilateral distinct wires were made in the FE models to simulate muscle fascicles (Figure 1d). Sixty-two bilateral fascicles of local muscles were attached to lumbar vertebrae (LGPL: longissimus thoracis pars lumborum; ICPL: iliocostalis lumborum pars lumborum; MFL: multifidus lumborum; MFT: multifidus thoracis; QL: quadratus lumborum; and IP: iliopsoas), and thirty bilateral fascicles of global muscles were connected to thoracic spine and cage, including global back muscles (LGPT: longissimus thoracis pars thoracic; and ICPT: iliocostalis lumborum pars thoracic), and global abdominal muscles (IO: internal oblique; EO: external oblique; and RA: rectus abdominus) [33]. (For interpretation of the references to color in this figure legend, the reader is referred to the web version of this article.)

loads at each level, applied eccentrically to the MS model, and muscles' physiological cross-sectional areas (PCSA) were used by scaling the magnitudes of the *in-vivo* measurements represented in the literature [34–38] (Fig. 2).

Muscle forces and reaction moments were estimated in the upright-standing posture using an optimization algorithm which was constrained to equilibrium and stability conditions [33,39]. The moment equilibrium equations were formulated by taking the CoR into account. Equation (1) was used to optimize the muscle stresses and reaction moments in the MS model to meet the stability condition in a scoliotic spine [39]. To address the redundancy in the system of equations, which includes 110 unknowns (92 muscle forces and 18 reaction moments) but only 18 equilibrium equations, i.e. 3 equality equations at each level for 6 joints, an

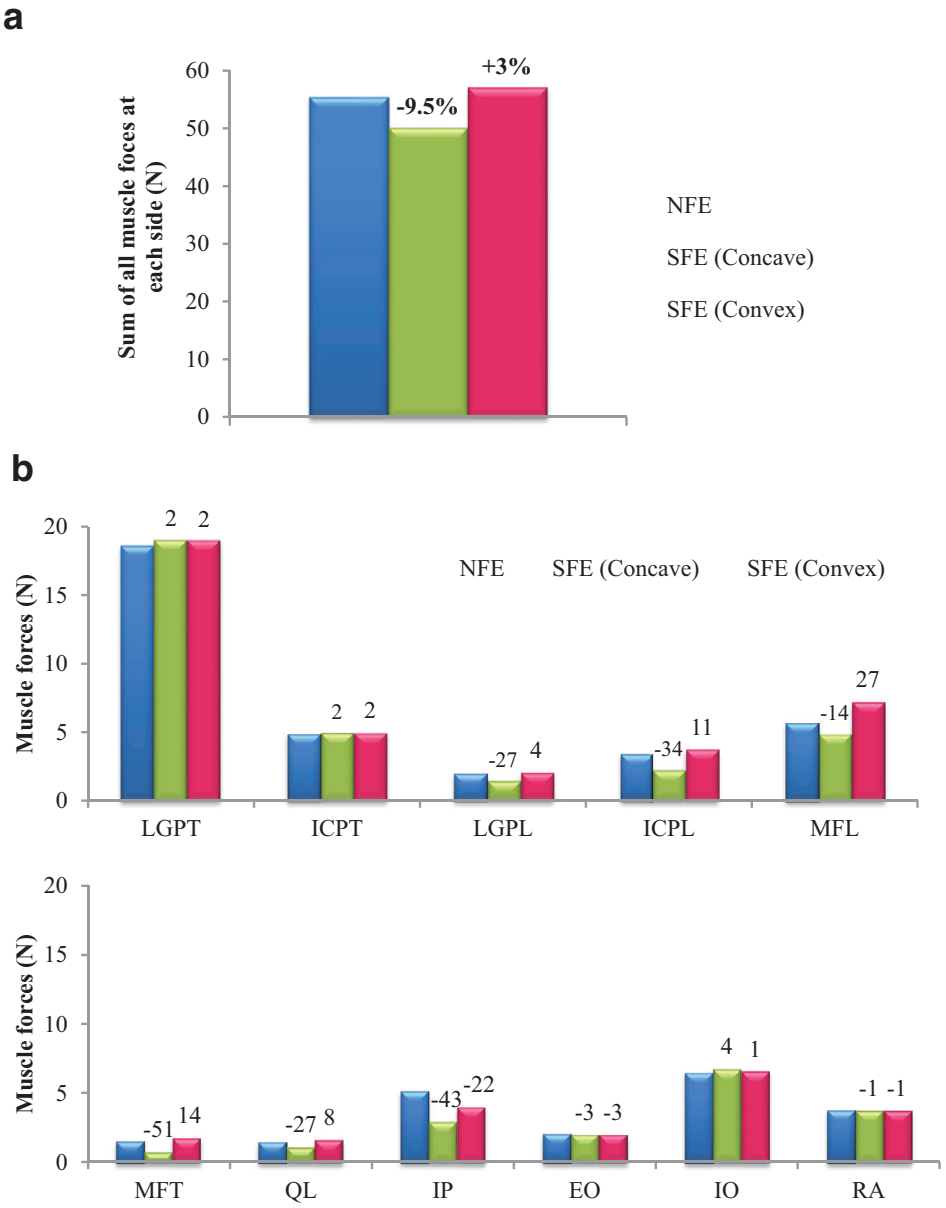

Figure 3. (a) Sum of all muscle forces in NFE and SFE models (N), and (b) individual muscle forces (N) of pediatric normal and scoliotic models of spine on each side of the spine, with the change percentage in the muscle forces over the FE models on each bar. The complete names of the muscles were appeared in Figure 2.

Table 2
Reaction moments (M^{CoR}) and the shift of the CoR from the IVD centroids (D^{CoR}) in local coordinates at each level in the SFE model. The directions were appeared in Figure 1.

Level	M^{CoR} (N.mm)			D^{CoR} (mm)		
	M^{CoR}_{ml}	M^{CoR}_{long}	M^{CoR}_{ap}	D^{CoR}_{ml}	D^{CoR}_{long}	D^{CoR}_{ap}
T12-L1	0.0	75.3	101.6	−0.7	0.0	0.0
L1-L2	−71.9	83.4	356.7	−1.0	0.0	−0.2
L2-L3	−158.5	116.8	653.7	−3.5	0.0	−0.8
L3-L4	−71.9	74.8	238.2	−1.2	0.0	−0.4
L4-L5	−30.4	64.1	60.3	−0.3	0.0	−0.2
L5-S1	0.0	49.6	33.0	−0.2	0.0	0.0

optimization algorithm was used in Matlab to minimize summation of the cubed muscle stresses and reaction moments. Equilibrium equations were written at six levels, i.e. T12-S1, to calculate muscle forces and reaction moments in the global *xyz* coordinate system (Fig. 1).

$$min\left(\sum_{m=1}^{92}\left(\frac{F_m}{A_m}\right)^n + Const.\left(\sum_{i=1}^{6}\left|M_{xi}^{CoR}\right|^n + \sum_{i=1}^{6}\left|M_{yi}^{CoR}\right|^n + \sum_{i=1}^{6}\left|M_{zi}^{CoR}\right|^n\right)\right)$$
$$subject\ to: \begin{cases} \sum M_i^{total} = M_i^{CoR} \quad i = 1, 2, \ldots, 18 \\ eig(Hessian) > 0 \\ F_{passive} \le F_m \le \sigma_{max}.A_m + F_{passive} \quad m = 1, \ldots, 92 \end{cases} \tag{1}$$

Equation (1) includes unknown individual forces for each muscle (F_m), the muscle PCSA (A_m), summation of all moments (M^{total}) and unknown reaction moments (M^{CoR}) at each joint about the center of the IVD in three directions, the passive force components ($F_{passive}$), the eigen-values of the Hessain matrix of the potential energy, *eig (Hessian)*, and maximum allowable muscle stress (σ_{max}) which was assumed to be 0.6 MPa [33]. To investigate the stress distribution within the GPs, the reaction forces (approximated as vector summation of the muscle and gravitational forces at each

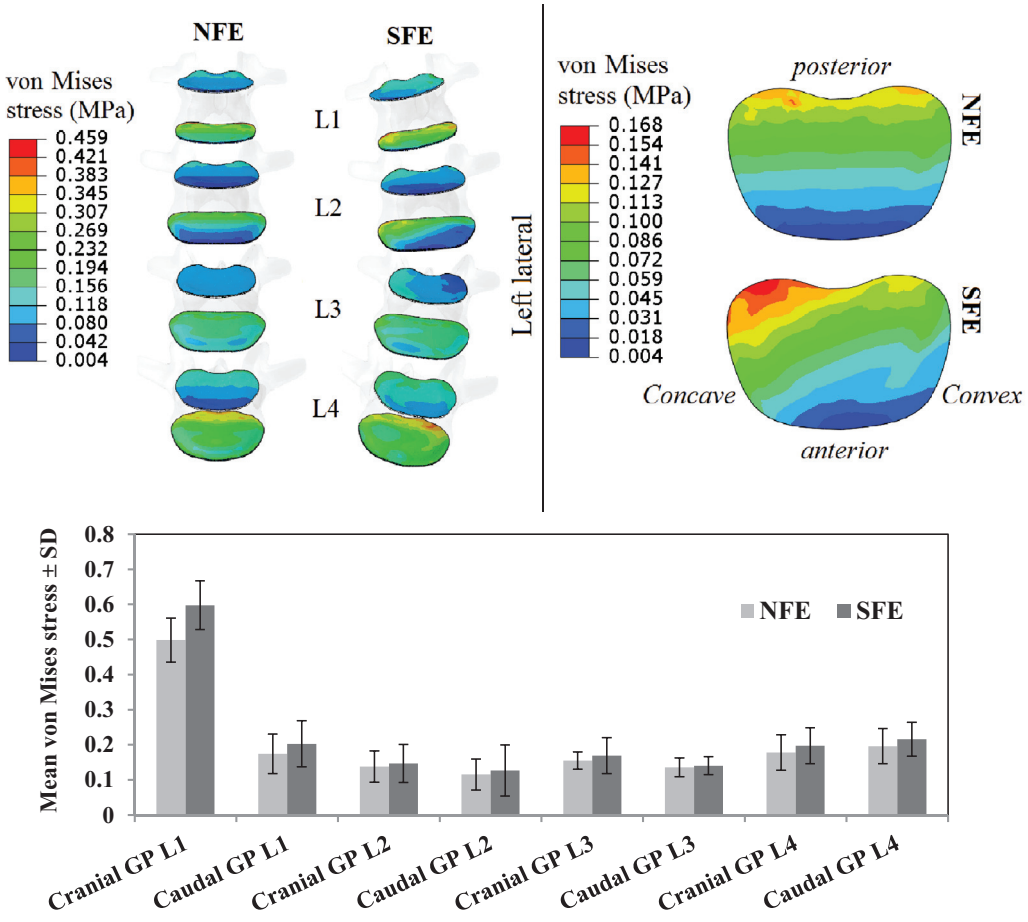

Figure 4. Results of von Mises stress distribution within: (Top left) the cranial and caudal GPs of L1 to the L4 vertebrae; (Top right) the load-sensitive area of the caudal GP of L2 in NFE and SFE models; and (Bottom) Mean and standard deviation (SD) of the von Mises stress at each GP of the NFE and SFE models.

level) as well as the reaction moments about the IVD centroids were applied on the load-sensitive areas of the cranial and caudal GPs of the fully-fixed L1 to L4 (Fig. 1e) as distributed pressures and shear stresses. Since the CoRs in the normal model were assumed to be at the IVD centroid [12–14], reaction moments about the IVD centroids in Equation (1) were used only in the case of the scoliotic model. The Matlab algorithm ensured that the results of the muscle forces and reaction moments were the global, rather than local, minimizers of the objective function shown in Equation (1).

2.3. Modeling bone growth and growth modulation

Measurements taken at monthly-intervals over a one year period were used to assess the deformity progression in the current study. Since bone growth is a long-term process, an average of daily-nightly loads [40] was assumed to be the mechanical stimulus on the spine. For the sake of simplification, daily loads included gravitational loads and muscle forces in an upright-standing position. Based on a ratio of nightly load to daily load (W_{night}/W_{day}) of about 0.35 [40], the average load on the spinal vertebrae was calculated using Equation (2) and applied on the FE models at each growth iteration.

$$W_{ave} = \frac{2}{3}W_{day} + \frac{1}{3}W_{night} = 78.3\%\ W_{day} \tag{2}$$

Stokes' model [41] (Eq. (3)), supported by *in-vivo* experimental data and evidence [42–45], was used to simulate the bone growth in this study.

$$\Delta\varepsilon_l = \Delta G_l(1 + \beta\sigma_l) \tag{3}$$

where the l-axis represents the longitudinal direction along the vertebral main axis and perpendicular to the growth plate. In Equation (3), the resulting growth strain increment $\Delta\varepsilon_l$ (month^{-1}) was expressed as the contribution of the baseline (physiological) longitudinal growth increment, ΔG_l (month^{-1}), which was adapted from the reported lumbar vertebrae growth rate of 1.1 mm/year [11] and a mechanically modulated growth increment, $\Delta G_l\beta\sigma_l$ (month^{-1}). The 2nd term was evaluated based on the internal mechanical stimulus, σ_l (MPa), and the sensitivity factor, β (MPa^{-1}) of bone tissue to that stimulus [41]. To calibrate the current growth model with the Stokes' model the parameters of the growth equation, Equation (3), were adjusted up until the average growth rate sensitivity to the stress was about 17.1%. This was done by adding the longitudinal stress $\Delta Stress = 0.1 MPa$, in two separate scenarios of distraction and compression, to the spinal loads on the vertebrae [42] (Eq. (4)).

$$Sensitivity = \frac{\Delta(Growth - Rate)\ \left(\frac{micron}{day}\right)}{\Delta Stress\ (MPa)} \tag{4}$$

where $\Delta(Growth - Rate)$ is the growth rate increment obtained by adding the $\Delta Stress$ to the stresses on the GPs.

Based on an experimentally determined range of 0.4∼1.71 MPa^{-1} for the sensitivity coefficient (β) [41,42,46] and 0.2∼1.2 mm/year for the baseline growth (G_l) [6,47,48] in the Stokes' model, sensitivity analyses were performed to assess the effects of β and G_l on the growth rates of the vertebrae and spine

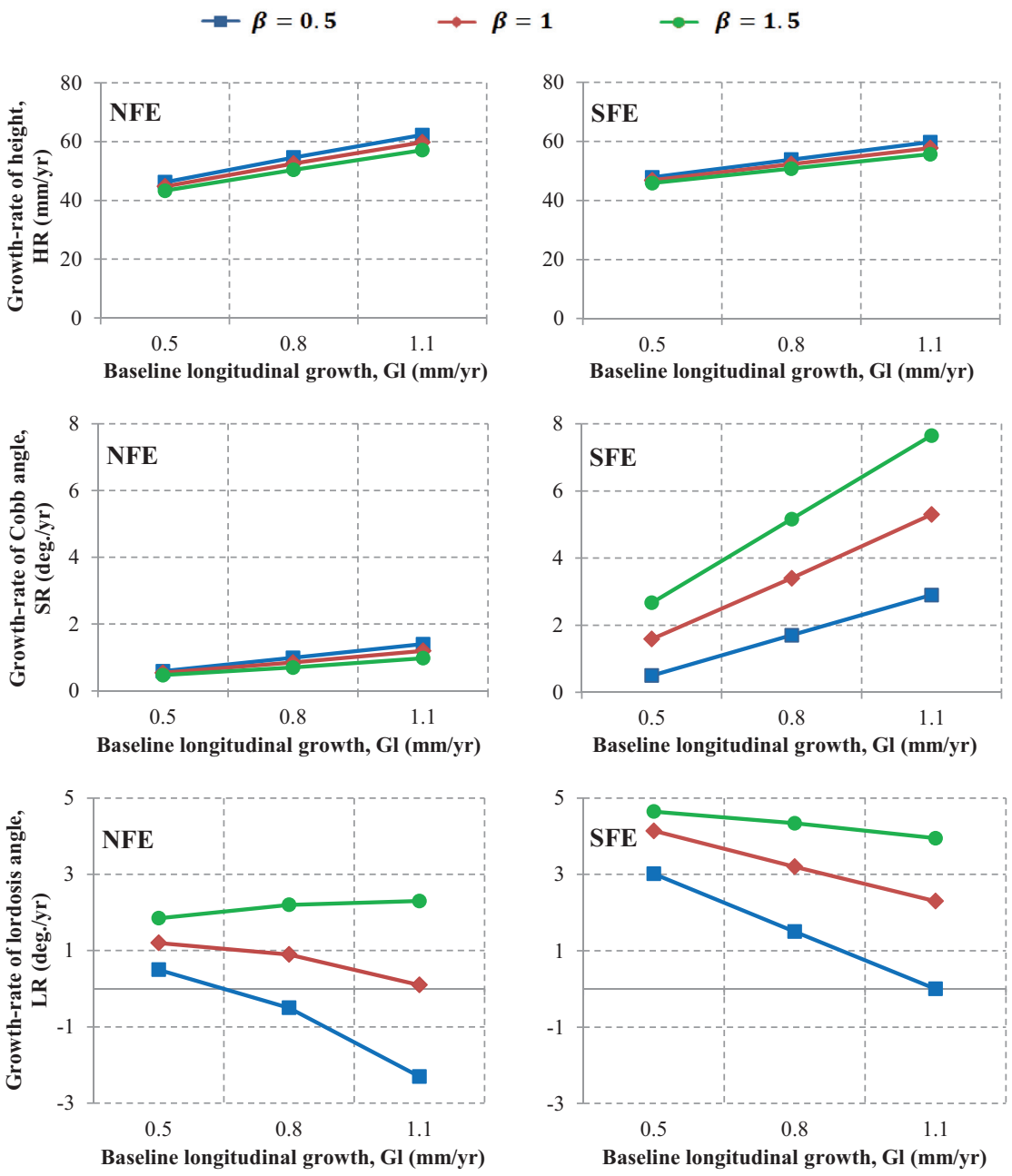

Figure 5. Predicted one-year growth rate of: (Top) the height (HR), in mm/year; (Middle) the scoliosis Cobb angle (SR); and (Bottom) the lordosis angle (LR), in deg./year, of the growing L1-L4 NFE compared to SFE model with different sensitivity coefficients, β, over the different values of baseline longitudinal growth, G_l, in the Stokes' model.

curvatures. To do so, different values of 0.5, 1, and 1.5 MPa^{-1} were chosen for the sensitivity coefficient (β) to compare with different baseline growth (G_l) values of 0.5, 0.8, and 1.1 mm/year in the Stokes' model [41]. Simulation of each iteration of the spine growth consisted of four consecutive steps: applying forces, measuring stresses in each element of the growth plates, calculating growth, and updating the geometry [4]. The Cobb angle, lordosis angle, and vertebral height of L1-L4 were calculated in each iteration.

3. Results

Asymmetric geometry of the scoliotic spine in the sagittal plane can cause asymmetry in the muscle forces, which in turn can put greater compression on one side leading to deformity progression. Results of this study showed that the sum of the muscle forces on the convex side of the scoliotic spine is greater than that of the concave side (Fig. 3a). The normalized difference shown on each bar (Fig. 3a) was calculated using Equation (5), in which A1 and A2 represent the sum of magnitudes of the forces of all muscles on each side of the NFE and SFE models, respectively:

$$\text{Normalized difference} = (A2 - A1)/(A1)(\%) \quad (5)$$

By dividing the vector summation of the gravity and muscle forces over the disc area at each level [49], with a correction factor of 0.66 [49], the intradiscal pressures at the L3-L4 and L4-L5 levels were found, respectively, to be ~0.32 and 0.38 MPa in the normal FE model and 0.30 and 0.36 MPa in the scoliotic FE model. Mean and standard deviation of the hydrostatic and octahedral shear stresses ($S_{ave} \pm SD$) in the apical GP, i.e. the caudal GP of the apex L2, were found, respectively, to be ~0.11 ± 0.05 and 0.05 ±

0.03 MPa in the NFE and ~0.11 ± 0.06 and 0.06 ± 0.04 MPa in the SFE model.

The CoRs shifted from the IVD centroids to the posteroconcave side in the SFE model (Table 2). The longitudinal shift of the CoR was negligible at all levels.

The FE analysis of the normal and scoliotic L1-L4 model under muscle forces, reaction moments, and gravity loads showed that the greatest difference between the stress levels in the concave and convex sides occurred in the apical GP in the SFE model, with a maximum SD of 7.3% (Fig. 4).

Using the Stokes' model with a sensitivity coefficient β of 1 MPa^{-1} and baseline physiological growth G_l of 1.1 mm/year [4], the total growth rates of scoliotic L1, L2, L3, and L4 were found to be ~12.9, 12.6, 16.4, and 17.0 mm/year, respectively. These were almost similar for the normal and scoliotic models. A positive correleation was found between the scoliotic spine height and Cobb angle growth rates for different values of the baseline growth and sensitivity coefficient of the Stokes' model (Fig. 5).

4. Discussion and conclusions

This study used a combination of musculoskeletal and finite element modeling to evaluate the stability-based muscle forces in a spine with adolescent idiopathic scoliosis compared to a normal spine, as well as to determine the effects of stress distribution within the growth plates of the growing spine under muscle exertions, reaction moments, and gravity loads. For this purpose nonlinear 3D FE models of the upright thoracolumbar spine of a scoliotic individual, consisting of cranial and caudal GPs attached to rigid L1 to L4 segments, were developed using CT images. The reaction forces, approximated as vector summation of the muscle and gravitational forces at each level, and the reaction moments about the IVD centroids were applied on the GPs of the fully-fixed L1 to L4, as an alternative to the *in-vivo* loading condition, to investigate the stress distribution within the GPs. Results of the present work showed the compatibility of the novel stability-constrained biomechanical trunk model to estimate muscle forces and reaction moments of an AIS spine, while integrating vertebral growth and growth modulation. Moreover, a sensitivity analysis was conducted on the effects of different values of the baseline physiological growth and sensitivity coefficient in the Stokes' model, i.e. G_l and β in Equation (3), on the growth pattern of the scoliotic spine.

Results of the scoliotic model (Fig. 3) showed that the cumulative force of the convex-side of the muscles was greater, on average by about 12.5%, than that of the contralateral muscles in agreement with the literature [50,51], with the greatest increase in the convex-side multifidus lumborum (MFL) force, i.e. by about 27% (Fig. 3b). Greater contraction of the convex-side para-spinal muscles (Fig. 3b) was consistent with previously reported greater electromyography activation of these muscles [52,53], indicating their important role in keeping the stability-based model of the AIS spine in equilibrium [54,55]. Moreover, it was also found that the maximum reaction moment can be found in the apical level of the SFE model (Table 2), where the farthest position of the off-centered CoR from the IVD centroid is located. The longitudinal reaction moment (Table 2) can induce an abnormal axial rotation in the AIS spine towards the concavity, which is a symptom that can identify idiopathic scoliosis [56,57]. It is also in agreement with the reported effect of the greater overall force of the convex-side muscles (Fig. 3a) on compelling the posterior parts of vertebral bodies' rotation towards the concave side [8,58].

In order to indirectly check the validity of the combined MS-FE models, the predicted muscle forces and reaction moments found in this study along with gravity loads were applied on each level of the fully-constrained L1-L4 FE models to estimate the intradiscal pressures. The IDPs at the L3-L4 and L4-L5 levels were, respectively, ~0.32 and 0.38 MPa in the normal FE model and 0.30 and 0.36 MPa in the scoliotic FE model, which are in satisfactory agreement with the *in-vivo* data in normal subjects ranging from 0.35–0.54 MPa [59–61] in the L4-L5 level and 0.27–0.33 MPa [62,63] in the L3-L4 level. Moreover, the mean and standard deviation of the hydrostatic and octahedral shear stresses in the caudal GP of apex L2 were found, respectively, to be ~0.11 ± 0.05 and 0.05 ± 0.03 MPa in the NFE and ~0.11 ± 0.06 and 0.06 ± 0.04 MPa in the SFE model, which were in agreement with another study [64] and comparable with the previously reported *in-vitro* experimental data of 0.31 and 0.03 MPa for hydrostatic and octahedral shear stresses in GP, respectively [13].

The greatest von Mises stress occurred in the apical GP of the SFE model (Fig. 4), with a maximum SD of 7.3% from the average von Mises stress in the same tissue. This observation reaffirmed the association between the maximum reaction moment and the greatest shift of the CoR away from the IVD centroid at the apex level (Table 2). The greater stress level on the posteroconcave side of the GPs (Fig. 4), due to the shift of the CoRs towards the same side (Table 2), can confine the bone growth rate in that region, and in turn can promote increasing spine deformity in accordance with the Hueter–Volkmann theory as well as anterior spinal overgrowth in AIS consistent with the literature [65,66].

Based on experimentally determined ranges [41,42,46–48], a complementary sensitivity analysis of the baseline physiological growth, G_l, (0.5–1.1 mm/year), and the sensitivity factor, β, (0.5–1.5 MPa^{-1}) in the Stokes' model, it was shown that these parameters have significant effects on the growth rate and curvature progression of the spine (Fig. 5). The positive correleation between the scoliotic spine height and Cobb angle growth rates (Fig. 5) is in agreement with the reported clinical effects of rapid spine growth on spine curvatures [67–70]. While increasing G_l amplified both the baseline and mechanically modulated growth rates obtained by the Stokes' model, the augmented β intensified only the effect of the mechanical stresses on the GP. While this led to an increase in the angle of curvatures of the spine and a reduction in the vertebral growth (Fig. 5), they both still remained in the physiological ranges [71]. The augmented baseline growth in the Stokes' model mostly increased the growth rates of the spine height and Cobb angle (Fig. 5); however, it decreased the lordosis angle with a slow continuous trend in agreement with another study [72]. Using Stokes' model [41] Equation (3) with a sensitivity coefficient, β, of 1 MPa^{-1} and baseline physiological growth, G_l, of 1.1 mm/year [4], the total growth rates of L1-L4 were found to be 12.6–17.0 mm/year, which were in agreement with the values of 6–32 mm/year at each spinal growth plate [48,73]. No significant difference was seen between the spine height growth rate of the normal and AIS models (Fig. 5), which is in agreement with the literature [70]. The produced coronal deviation in the normal growing spine (Fig. 5) reinforced the hypothesis which states that a primary disorder in the spine is a key factor in the AIS progression [74], and is consistent with the mild trunk asymmetries observed in healthy adolescents in school screening [75–78].

Due to the lack of data in the current literature, the scoliotic model in this study was validated against a normal spine. Noting the capability of the Stokes' model [41] to predict bone longitudinal growth [14], the transverse growth of bone and consequent vertebral physiological cross-sectional area changes were not taken into account in this work. The growth of muscles was indirectly accounted for by changing their attachment sites during growth, as suggested in the literature [79]. In addition, the gravitational loads and PCSA of the muscles were used by scaling the magnitudes of the *in-vivo* measurements represented in the literature [34-38]. Moreover, assuming that the deformity in AIS is mostly associated with the disturbed endochondral growth of the vertebral

body rather than that of the posterior elements [66,80], the growth of the posterior elements was not considered here either. It should be noted that besides biomechanical stimuli there are many other factors, such as neurological, evolutionary, genetic, environmental, and hormonal factors [81–84], at play and effective in the development of spine deformity. However, in the current study the growth of the scoliotic spine was investigated by only biomechanical factors.

In conclusion, two staggered FE-MS models of one normal and one scoliotic trunk, each coupled with a growth modulation, were investigated using a stability-based optimization approach in order to predict the growth rates of the vertebrae height and spine curvatures using different parameter values in the Stokes' growth model [41]. The approach presented in this study might be used to investigate the effects of long-term strengthening of the muscles and alignment correction exercises in order to devise more effective plans for conservative clinical therapies, such as exercise therapy or bracing, for patients with AIS. Due to the rib's protection and thus the semi-rigid behavior of the thoracic cage, the growth of the lumbar vertebrae should be more influenced by muscle exertions than that of the thoracic spine. Moreover, the lumbar spine is more exposed to the risk of loss of stability than the thoracic spine [85] and thus has a greater potential of deformity progression than the thorax [86]. These notions may encourage one to conclude that despite the reportedly more severe evolution of thoracic scoliosis [87], the lumbar spine rather than the thoracic spine might be a better candidate to investigate the effects of muscular therapies on scoliotic spine stability. It is hoped that the stability-based model of the AIS spine presented here can be employed to increase our understanding of the complex mechanisms involved in scoliotic progression, and to help researchers in their investigations of the performance of therapeutic devices, such as growing rods, to improve the design of preventive rehabilitation strategies for the clinical management of AIS.

Funding

This work was supported by grants from Amirkabir University of Technology (Tehran, Iran), and the University of Alberta (Alberta, Canada).

Ethical approval

The collection and use of patient-specific CT and EOS images on which this study is based were approved by the Ethics Committee of Shahid Sadooghi Hospital (Yazd, Iran).

Conflict of interest

The authors have no conflicts of interest relevant to this article to report.

Acknowledgment

This work was supported by grants from Amirkabir University of Technology (Tehran, Iran), and the University of Alberta (Alberta, Canada). The authors would also like to appreciate Dr. Eric Parent, Faculty of Rehabilitation Medicine at the University of Alberta, for his critical review and useful comments.

References

[1] Wajchenberg M, Astur N, Kanas M, Martins DE. Adolescent idiopathic scoliosis: current concepts on neurological and muscular etiologies. Scoliosis Spinal Disord 2016;11:4.
[2] Castelein RM. Pre-existent rotation of the normal spine at different ages and its consequences for the scoliotic mechanism. Stud Health Technol Inform 2012;176:20–5.
[3] Trobisch P, Suess O, Schwab F. Idiopathic Scoliosis. Dtsch Arztebl Int 2010;107(49):875–83.
[4] Lin H, Aubin CE, Parent S, Villemure I. Mechanobiological bone growth: comparative analysis of two biomechanical modeling approaches. Med Biol Eng Comput 2009;47(4):357–66.
[5] Sevrain A, Aubin CE, Gharbi H, Wang X, Labelle H. Biomechanical evaluation of predictive parameters of progression in adolescent isthmic spondylolisthesis: a computer modeling and simulation study. Scoliosis 2012;7:2.
[6] Abolaeha OA. Smart growing rod device for the treatment of early onset scoliosis Ph.D. thesis. University of Dayton; 2010.
[7] Agarwal A, Agarwal AK, Jayaswal A, Goel VK. Effect of distraction force on growth and biomechanics of the spine: a finite element study on normal juvenile spine with dual growth rod instrumentation. Spine deform 2014; 2(4):260–9.
[8] Maryse F. Paraspinal muscle morphology, composition and asymmetries: determinants and relation to low back pain and pathology Ph.D. thesis. University of Alberta; 2013.
[9] Rose A, Breen A. Relationships between paraspinal muscle activity and lumbar inter-vertebral range of motion. Healthcare (Basel) 2016;4(1):4.
[10] Azari F, Arjmand N, Shirazi-Adl A, Rahimi-Moghaddam T. A combined passive and active musculoskeletal model study to estimate L4-L5 load sharing. J Biomech 2018;70:157–65.
[11] Huynh AM, Aubin CE, Mathieu PA, Labelle H. Simulation of progressive spinal deformities in Duchenne muscular dystrophy using a biomechanical model integrating muscles and vertebral growth modulation. Clin Biomech 2007;22(4):392–9.
[12] Arjmand N, Gagnon D, Plamondon A, Shirazi-Adl A, Larivière C. Comparison of muscle forces and spinal loads estimated by two biomechanical models of the human trunk. Clin Biomech 2009;24:533–41.
[13] Gao J, Williams JL, Roan E. On the state of stress in the growth plate under physiologic compressive loading. OJBIPHY 2014;4(1):13–21.
[14] Stokes IA. Mechanical effects on skeletal growth. J Musculoskelet Neuronal Interact 2002;2(3):277–80.
[15] Mehlman C, Araghi A, Roy DR. Hyphenated history: the Hueter–Volkmann law. Am J Orthop (Belle Mead NJ) 1997;26(11):798–800.
[16] Andriacchi T, Schultz A, Belytschko T, Galante J. A model for studies of mechanical interaction between the human spine and rib cage. J Biomech 1974;7(6):497–507.
[17] Chaffin DB, Redfern MS, Erig M, Goldstein SA. Lumbar muscle size and locations from CT scans of 96 women of age 40 to 63 years. Clin Biomech (Bristol, Avon) 1990;5(1):9–16.
[18] Dumas GA, Poulin MJ, Roy B, Gagnon M, Jovanovic M. A three dimensional digitization method to measure trunk muscle lines of action. Spine (Phila Pa 1976) 1988;13(5):532–41.
[19] Dumas GA, Poulin MJ, Roy B, Gagnon M, Jovanovic M. Orientation and moment arms of some trunk muscles. Spine (Phila Pa 1976) 1991;16(3):293–303.
[20] McGill SM, Patt N, Norman RW. Measurement of the trunk musculature of active males using CT scan radiography: implications for force and moment generating capacity about L4/L5 joint. J Biomech 1988;21(4):329–41.
[21] Moga PJ, Erig MS, Chaffin DB, Nussbaum MA. Torso muscle moment arms at intervertebral levels T10 through L5 from CT scans on eleven male and eight female subjects. Spine (Phila Pa 1976) 1993;18(15):2305–9.
[22] Hui SC, Pialasse JP, Wong JY, Lam TP, Ng BK, Cheng JC, Chu WC. Radiation dose of digital radiography (DR) versus micro-dose x-ray (EOS) on patients with adolescent idiopathic scoliosis. Scoliosis Spinal Disord 2016;11:46.
[23] Modi HN, Suh SW, Song HR, Yang JH, Kim HJ, Modi CH. Differential wedging of vertebral body and intervertebral disc in thoracic and lumbar spine in adolescent idiopathic scoliosis–A cross sectional study in 150 patients. Scoliosis 2008;3:11.
[24] Sylvestre PL, Villemure I, Aubin CE. Finite element modeling of the growth plate in a detailed spine model. Med Biol Eng Comput 2007;45(10):977–88.
[25] Kamal Z, Rouhi G. A parametric investigation of the effects of cervical disc prostheses with upward and downward nuclei on spine biomechanics. J Mech Med Biol 2016;16(7):1650092.
[26] Campbell JQ, Coombs DJ, Rao M, Rullkoetter PJ, Petrella AJ. Automated finite element meshing of the lumbar spine: verification and validation with 18 specimen-specific models. J Biomech 2016;49(13):2669–76.
[27] Parashar SK, Sharma JK. A review on application of finite element modelling in bone biomechanics. Perspect Sci 2016;8:696–8.
[28] Dreischarf M, Zander T, Shirazi-Adl A, Puttlitz CM, Adam CJ, Chen CS, Goel VK, Kiapour A, Kim YH, Labus KM, Little JP, Park WM, Wang YH, Wilke HJ, Rohlmann A, Schmidt H. Comparison of eight published static finite element models of the intact lumbar spine: Predictive power of models improves when combined together. J Biomech 2014;47(8):1757–66.
[29] Little JP, Adam CJ, Evans JH, Pettet GJ, Pearcy MJ. Nonlinear finite element analysis of anular lesions in the L4/5 intervertebral disc. J Biomech 2007;40(12):2744–51.
[30] Moramarco V, Pérez del Palomar A, Pappalettere C, Doblaré M. An accurate validation of a computational model of a human lumbosacral segment. J Biomech 2010;43(2):334–42.
[31] Rao M. Explicit finite element modeling of the human lumbar spine Ph.D. thesis. University of Denver; 2012.
[32] Schmidt H, Kettler A, Heuter F, Claes L, Wilke HJ. Intradiscal pressure, shear strain, and fiber strain in the intervertebral disc under combined loading. Spine (Phila Pa 1976) 2007;32(7):748–55.

[33] Hajihosseinali M, Arjmand N, Shirazi-Adl A, Farahmand F, Ghiasi MS. A novel stability and kinematics-driven trunk biomechanical model to estimate muscle and spinal forces. Med Eng Phys 2014;36(10):1296–304.
[34] Arjmand N, Gagnon D, Plamondon A, Shirazi-Adl A, Lariviere C. A comparative study of two trunk biomechanical models under symmetric and asymmetric loadings. J Biomech 2010;43(3):485–91.
[35] Pearsall DJ. Segmental inertial properties of the human trunk as determined from computer tomography and magnetic resonance imagery (Ph.D. thesis). Kingston: Queen's University; 1994.
[36] de Leva P. Adjustments to Zatsiorsky–Seluyanov's segment inertia parameters. J Biomech 1996;29(9):1223–30.
[37] Bogduk N, Macintosh JE, Pearcy MJ. A universal model of the lumbar back muscles in the upright position. Spine (Phila Pa 1976) 1992;17(8):897–913.
[38] Stokes IA, Gardner-Morse M. Quantitative anatomy of the lumbar musculature. J Biomech 1999;32(3):311–16.
[39] Cholewicki J, McGill SM. Mechanical stability of the in vivo lumbar spine: implications for injury and chronic low back pain. Clin Biomech (Bristol, Avon) 1996;11(1):1–15.
[40] Schmidt H, Shirazi-Adl A, Galbusera F, Wilke HJ. Response analysis of the lumbar spine during regular daily activities—A finite element analysis. J Biomech 2010;43(10):1849–56.
[41] Stokes IA, Laible JP. Three-dimensional osseo-ligamentous model of the thorax representing initiation of scoliosis by asymmetric growth. J Biomech 1990;23(6):589–95.
[42] Stokes IA, Aronsson DD, Dimock AN, Cortright V, Beck S. Endochondral growth in growth plates of three species at two anatomical locations modulated by mechanical compression and tension. J Orthop Res 2006;24(6):1327–34.
[43] Stokes IA, Gwadera J, Dimock A, Farnum CE, Aronsson DD. Modulation of vertebral and tibial growth by compression loading: diurnal versus full-time loading. J Orthop Res 2005;23(1):188–95.
[44] Stokes IA, Clark KC, Farnum CE, Aronsson DD. Alterations in the growth plate associated with growth modulation by sustained compression or distraction. Bone 2007;41(2):197–205.
[45] Stokes IA, Mente PL, Latridis JC, Farnum CE, Aronsson DD. Enlargement of growth plate chondrocytes modulated by sustained mechanical loading. J Bone Joint Surg Am 2002;84-A(10):1842–8.
[46] Carrier J, Aubin CE, Villemure I, Labelle H. Biomechanical modelling of growth modulation following rib shortening or lengthening in adolescent idiopathic scoliosis. Med Biol Eng Comput 2004;42(4):541–8.
[47] Stokes IA, Spence H, Aronsson DD, Kilmer N. Mechanical modulation of vertebral body growth. Implications for scoliosis progression. Spine (Phila Pa 1976) 1996;21(10):1162–7.
[48] Stokes IA. Analysis and simulation of progressive adolescent scoliosis by biomechanical growth modulation. Eur Spine J 2007;16(10):1621–8.
[49] Dreischarf M, Rohlmann A, Zhu R, Schmidt H, Zander T. Is it possible to estimate the compressive force in the lumbar spine from intradiscal pressure measurements? A finite element evaluation. Med Eng Phys 2013;35(9):1385–90.
[50] Freeman MD, Woodham MA, Woodham AW. The role of the lumbar multifidus in chronic low back pain: a review. Pm R 2010;2(2):142–6.
[51] Chan YL, Cheng JCY, Guo X, King AD, Griffith JF, Metreweli C. MRI evaluation of multifidus muscles in adolescent idiopathic scoliosis. Pediatr Radiol 1999;29:360–3.
[52] Cheung J, Veldhuizen AG, Halberts JP, Sluiter WJ, Van Horn JR. Geometric and electromyographic assessments in the evaluation of curve progression in idiopathic scoliosis. Spine (Phila Pa 1976) 2006;31(3):322–9.
[53] Alves DPLA, Araújo B. Muscle disorders in adolescent idiopathic scoliosis: literature review. Coluna/Columna 2016;15(1):73–7.
[54] Stokes IA, Gardner-Morse MG, Henry SM. Abdominal muscle activation increases lumbar spinal stability: analysis of contributions of different muscle groups. Clin Biomech (Bristol, Avon) 2011;26(8):797–803.
[55] Zuk T. The role of spinal and abdominal muscles in the pathogenesis of scoliosis. J Bone Joint Surg 1962;44-B(1):102–5.
[56] Eyvazov K, Samartzis D, Cheung JPY. The association of lumbar curve magnitude and spinal range of motion in adolescent idiopathic scoliosis: a cross-sectional study. BMC Musculoskelet Disord 2017;18:51.
[57] Hefti F. Pathogenesis and biomechanics of adolescent idiopathic scoliosis (AIS). J Child Orthop 2013;7(1):17–24.
[58] Lam GC, Hill DL, Le LH, Raso JV, Lou EH. Vertebral rotation measurement: a summary and comparison of common radiographic and CT methods. Scoliosis 2008;3:16.
[59] Wilke HJ, Neef P, Caimi M, Hoogland T, Claes LE. New in vivo measurements of pressures in the intervertebral disc in daily life. Spine (Phila Pa 1976) 1999;24(8):755–62.
[60] Sato K, Kikuchi S, Yonezawa T. In vivo intradiscal pressure measurement in healthy individuals and in patients with ongoing back problems. Spine (Phila Pa 1976) 1999;24(23):2468–74.
[61] Takahashi I, Kikuchi S, Sato K, Sato N. Mechanical load of the lumbar spine during forward bending motion of the trunk—a biomechanical study. Spine (Phila Pa 1976) 2006;31(1):18–23.
[62] Schultz A, Andersson G, Ortengren R, Haderspeck K, Nachemson A. Loads on the lumbar spine. Validation of a biomechanical analysis by measurements of intradiscal pressures and myoelectric signals. J Bone Joint Surg Am 1982;64(5):713–20.
[63] Nachemson A, Elfström G. Intravital dynamic pressure measurements in lumbar discs. A study of common movements, maneuvers and exercises. Scand J Rehabil Med Suppl 1970;1:1–40.
[64] Piszczatowski S. Material aspects of growth plate modelling using Carter's and Stokes's approaches. Acta Bioeng Biomech 2011;13(3):3–14.
[65] Schlösser TP, van Stralen M, Chu WC, Lam TP, Ng BK, Vincken KL, Cheng JCY, Castelein RM. Anterior overgrowth in primary curves, compensatory curves and junctional segments in adolescent idiopathic scoliosis. PLoS One 2016;11(7):e0160267.
[66] Guo X, Chau WW, Chan YL, Cheng JC, Burwell RG, Danger field PH. Relative anterior spinal overgrowth in adolescent idiopathic scoliosis–result of disproportionate endochondral-membranous bone growth? Summary of an electronic focus group debate of the IBSE. Eur Spine J 2005;14(9):862–73.
[67] Shi B, Mao S, Liu Z, Sun X, Zhu Z, Zhu F, Cheng JCY, Qiu Y. Spinal growth velocity versus height velocity in predicting curve progression in peri-pubertal girls with idiopathic scoliosis. BMC Musculoskelet Disord 2016;17(1):368.
[68] Escalada F, Marco E, Duarte E, Ma Muniesa J, Boza R, Tejero M, Cáceres E. Assessment of angle velocity in girls with adolescent idiopathic scoliosis. Scoliosis 2009;4:20.
[69] Nissinen M, Heliövaara M, Seitsamo J, Poussa M. Trunk asymmetry, posture, growth, and risk of scoliosis. A three-year follow-up of Finnish prepubertal school children. Spine (Phila Pa 1976) 1993;18(1):8–13.
[70] Skogland LB, Miller JA. The length and proportions of the thoracolumbar spine in children with idiopathic scoliosis. Acta Orthop Scand 1981;52(2):177–185.
[71] Rogol AD, Clark PA, Roemmich JN. Growth and pubertal development in children and adolescents: effects of diet and physical activity. Am J Clin Nutr 2000;72(2 Suppl) 521S-528S.
[72] Shi L, Wang D, Driscoll M, Villemure I, Chu WCW, Cheng JCY, Aubin CE. Biomechanical analysis and modeling of different vertebral growth patterns in adolescent idiopathic scoliosis and healthy subjects. Scoliosis 2011;6:11.
[73] Mavrych V, Bolgova O, Ganguly P, Kashchenko S. Age-related changes of lumbar vertebral body morphometry. Austin J Anat 2014;1(3):1014.
[74] Dayer R, Haumont T, Belaieff W, Lascombes P. Idiopathic scoliosis: etiological concepts and hypotheses. J Child Orthop 2013;7(1):11–16.
[75] Grivas TB, Vasiliadis ES, Koufopoulos G, Segos D, Triantafyllopoulos G, Mouzakis V. Study of trunk asymmetry in normal children and adolescents. Scoliosis 2006;1:19.
[76] Burwell RG, James NJ, Johnson F, Webb JK, Wilson YG. Standardized trunk asymmetry scores–a study of back contour in healthy children. J Bone Joint Surg Br 1983;65(4):452–63.
[77] Vercauteren M, Van Beneden M, Verplaetse R, Croene P, Uyttendaele D, Verdonk R. Trunk asymmetries in a belgian school population. Spine (Phila Pa 1976) 1982;7(6):555–62.
[78] Balla BJ, Hanțiu I. Study on trunk asymmetry in children aged 10–15 years. Studia Ubb Educatio Artis Gymn 2016;61(2):15–24.
[79] Villemure I, Aubin CE, Dansereau J, Labelle H. Simulation of progressive deformities in adolescent idiopathic scoliosis using a biomechanical model integrating vertebral growth modulation. J Biomech Eng 2002;124(6):784–90.
[80] Xiong B, Sevastik J, Hedlund R, Sevastik B. Sagittal configuration of the spine and growth of the posterior elements in early scoliosis. J Orthop Res 1994;12(1):113–18.
[81] Fadzan M, Bettany-Saltikov J. Etiological theories of adolescent idiopathic scoliosis: past and present. Open Orthop J 2017;11:1466–89.
[82] Luo HJ, Lin SX, Wu SK, Tsai MW, Lee SJ. Comparison of segmental spinal movement control in adolescents with and without idiopathic scoliosis using modified pressure biofeedback unit. PLoS One 2017;12(7):e0181915.
[83] Aubin CÉ, Clin J, Rawlinson J. Biomechanical simulations of costo-vertebral and anterior vertebral body tethers for the fusionless treatment of pediatric scoliosis. J Orthop Res 2018;36(1):254–64.
[84] Schlager B, Niemeyer F, Galbusera F, Wilke HJ. Asymmetrical intrapleural pressure distribution: a cause for scoliosis? A computational analysis. Eur J Appl Physiol 2018;118(7):1315–29.
[85] Bergmark A. Stability of the lumbar spine. A study in mechanical engineering. Acta Orthop Scand Suppl 1989;230:1–54.
[86] Pesenti S, Jouve JL, Morin C, Wolff S, Sales de Gauzy J, Chalopin A, Ibnoulkhatib A, Polirsztok E, Walter A, Schuller S, Abelin-Genevois K, Leroux J, Lechevallier J, Kabaj R, Mary P, Fuentes S, Parent H, Garin C, Bin K, Peltier E, Blondel B, Chopin D. Evolution of adolescent idiopathic scoliosis: results of a multicenter study at 20 years' follow-up. Orthop Traumatol Surg Res 2015;110(5):619–22.
[87] Kenneth AO. Examination and treatment of thoracic spine disorders. In: Kenneth AO. Manual physical therapy of the spine. Elsevier Ltd; 2009. p. 199–246.